Simulation-Based Investigation of Crack Formation in Forged MB15 Magnesium Alloy

Lulu Song[1], Dongmei Liu[1], Jie Yuan[1], Ruihuan Tian[1], Liying Jin[2]*

[1]Metrological Physics and Chemistry Center, AVIC Aerospace Life-Support Industries, Ltd., Xiangyang 441003, Hubei Province, China
[2]Xiangyang Key Laboratory of Intelligent Manufacturing and Machine Vision, Hubei University of Arts and Science, Xiangyang 441053, Hubei Province, China

Corresponding author: Liying Jin, JLY@hbuas.edu.cn

Abstract: In the process of riveting an MB15 forging die, cracks were discovered emerging along the longitudinal direction and near the riveting hole. Through fracture analysis, microscopic observation, energy spectrum analysis, metallographic examination, and hardness test, the properties and causes of the cracks are discussed. The results indicate that the cracking type is intergranular brittle cracking, occurring during the forging stage. Furthermore, the recrystallization at the crack site is found to be incomplete, which is attributed to the low deformation temperature.

Keywords: MB15; Forging die; Crack; Deformation temperature

1. Introduction

MB15 is a high-strength deformed magnesium alloy belonging to the magnesium-zinc-zirconium series, capable of being strengthened through heat treatment. The process properties of this alloy, with lower plasticity compared to the medium-strength MB2, MB3, and MB8 alloys, resulted in a limited production range, mainly focused on extruded products, forgings, and forging dies. The alloy finds primary applications in the production of aircraft girders, rocker arms in the operating system, supports, and other stress components [1].

During the assembly and riveting of a batch of MB15 deformed magnesium alloy forgings, cracks were discovered along the longitudinal axis and near the riveting holes. The production process involves heating the bar die, forging and pressing the billet, milling the billet die, heating the billet die, two forging forming, grinding the flash, heat treatment, surface treatment, lettering, machine addition, surface oxidation, painting, and assembly. Through macroscopic observation, microscopic observation, energy spectrum analysis, metallographic inspection, and hardness test of the crack fracture, the properties and causes of the crack are discussed.

2. Test process

2.1. Macroscopic observation

After undergoing chemical oxidation and paint treatment, the forging surface appears black. Cracks are distributed parallel to the forging flow line, with some penetrating the entire thickness from the outer wall, while others do not. These cracks exhibit a flat and straight nature, and local positions reveal the presence of multiple cracks, as depicted in **Figure 1**.
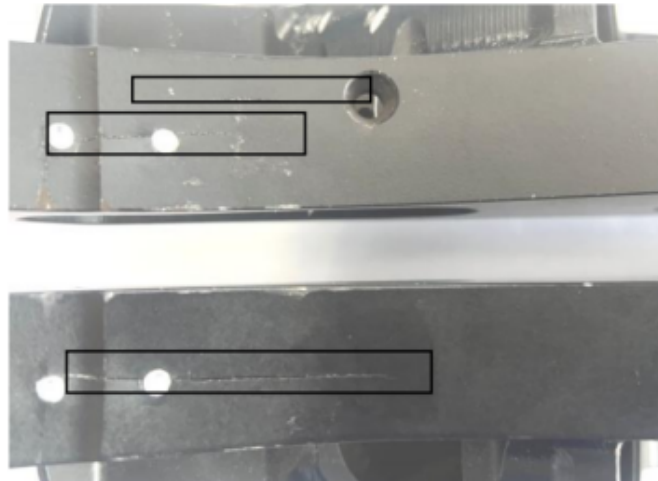
Figure 1. Macroscopic morphology of cracks

For macroscopic observation, the crack location was manually opened. Cracks extend from the outer wall towards the interior, resulting in relatively level fractures. The original crack area appears dark gray, and the local crack area exhibits a yellowish-brown tint with a noticeable small step characteristic. The artificially interrupted fracture appears silver-gray, as illustrated in **Figure 2**. The original cracked area and artificially interrupted area were observed respectively under stereomicroscope, and the step characteristics and reflective features were visible in the original cracked area, as shown in **Figure 2**. The fracture in the artificially interrupted area was fibrous, as shown in **Figure 2**.


Figure 2. Macroscopic morphology of the fracture

2.2. Microscopic observation

The crack fracture was examined under a scanning electron microscope (SEM). In the initial crack zone, the fractures appeared flush, covered with a substantial amount of oxides. Local, clear intergranular characteristics were observed, and no metallurgical defects were present, as illustrated in **Figure 3(a)**. During the middle stage of expansion, the fracture exhibited evenness, displaying layered cracking characteristics. Upon magnification,
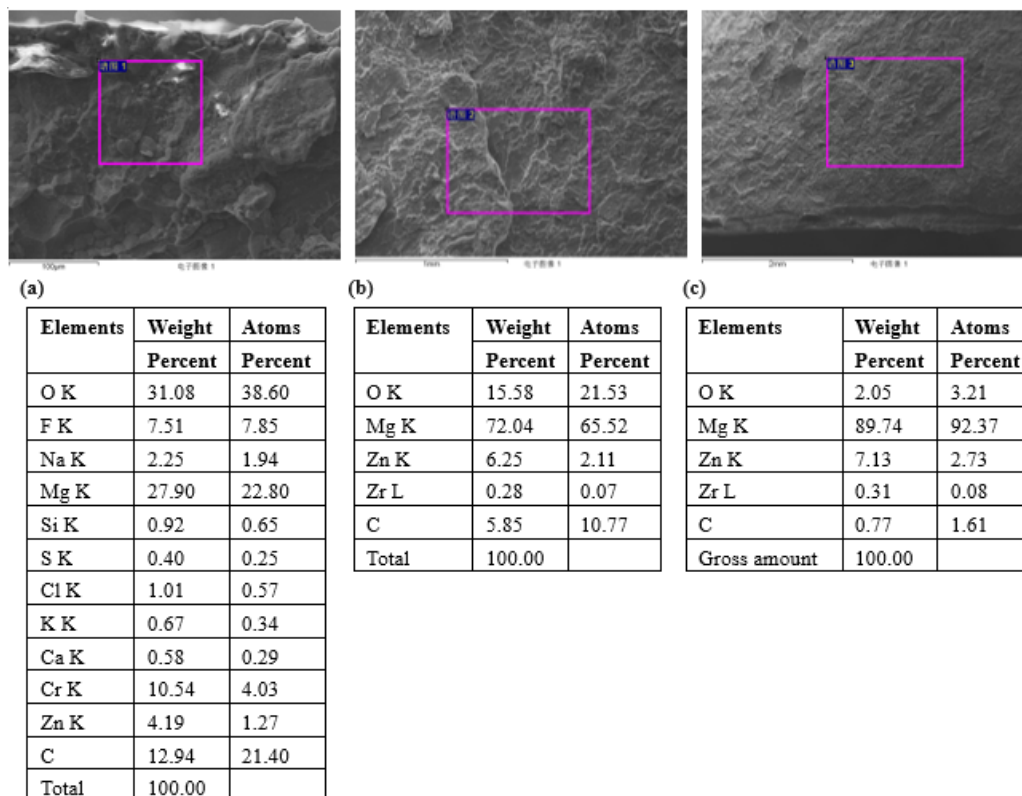
the fracture was found to be intergranular, with noticeable oxide adhesion on the crystal surface, as depicted in **Figure 3(b)**. The characteristics of fractures at the end stage of the expansion were similar to the middle stage, showing intergranular with the crystal surface exhibiting oxidation, as shown in **Figure 3(c)**. Fractures resulting from artificial interruption displayed cleavage-like features, as depicted in **Figure 3(d)**.
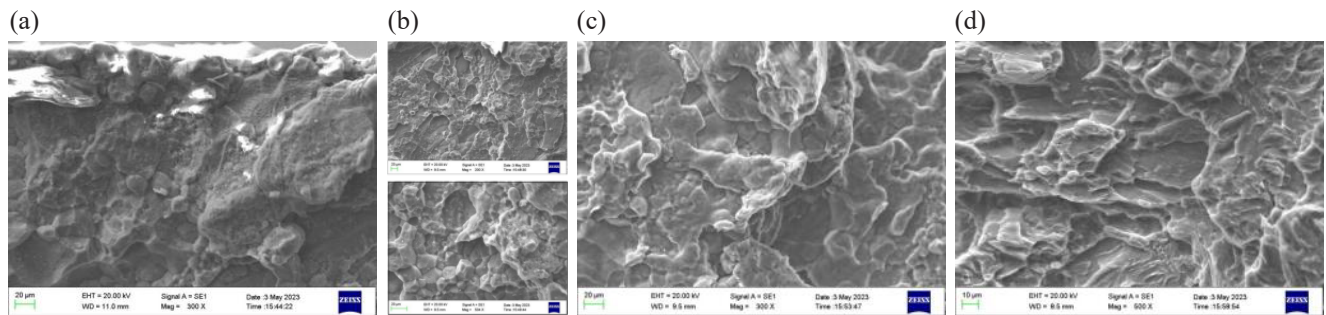
Figure 3. Microscopic observation of the crack fracture. **(a)** Initial cracking zone; **(b)** Middle stage of expansion; **(c)** End stage of expansion; **(d)** Artificial interruption of the fracture

2.3. Energy spectrum analysis

The crack's source region, expansion region, and artificially induced fracture region were analyzed separately. In the crack source region, additional elements such as O, F, Na, and Cr were identified. Elements such as F, Na, and Cr originated from chemical oxidation, with the surface crack fracturing during this process, as illustrated in **Figure 4(a)**. The expansion zone exhibited a higher concentration of O elements, while the types and contents of the main alloy elements essentially met the requirements of the MB15 alloy, as shown in **Figure 4(b)**. In the artificially induced fracture, the O element content was significantly reduced due to natural oxidation, yet the types and contents of the primary alloy elements met the specifications of the MB15 alloy, as depicted in **Figure 4(c)**.

Elements	Weight Percent	Atoms Percent
O K	31.08	38.60
F K	7.51	7.85
Na K	2.25	1.94
Mg K	27.90	22.80
Si K	0.92	0.65
S K	0.40	0.25
Cl K	1.01	0.57
K K	0.67	0.34
Ca K	0.58	0.29
Cr K	10.54	4.03
Zn K	4.19	1.27
C	12.94	21.40
Total	100.00	

Elements	Weight Percent	Atoms Percent
O K	15.58	21.53
Mg K	72.04	65.52
Zn K	6.25	2.11
Zr L	0.28	0.07
C	5.85	10.77
Total	100.00	

Elements	Weight Percent	Atoms Percent
O K	2.05	3.21
Mg K	89.74	92.37
Zn K	7.13	2.73
Zr L	0.31	0.08
C	0.77	1.61
Gross amount	100.00	

Figure 4. Energy spectrum analysis of the crack. **(a)** Source area; **(b)** Expansion area; **(c)** Artificial interruption area

2.4. Metallographic analysis

Metallographic structure detection was performed at both the crack location and the intact location. It was observed that the cracks primarily propagated along the crystals, demonstrating good alignment between the two sides of the cracks. Simultaneously, a substantial number of elongated deformed grains and deformation bands were evident, with occasional occurrences of equiaxed crystals in local areas, as illustrated in **Figure 5(a)**. During the expansion stage, secondary cracks appeared on both sides of the main crack, extending along the crystal structure, as depicted in **Figure 5(b)**. No signs of overheating or overburning were observed in the structure. The normal position's metallographic structure morphology is presented in **Figure 5(c)**.

(a)   (b)   (c)
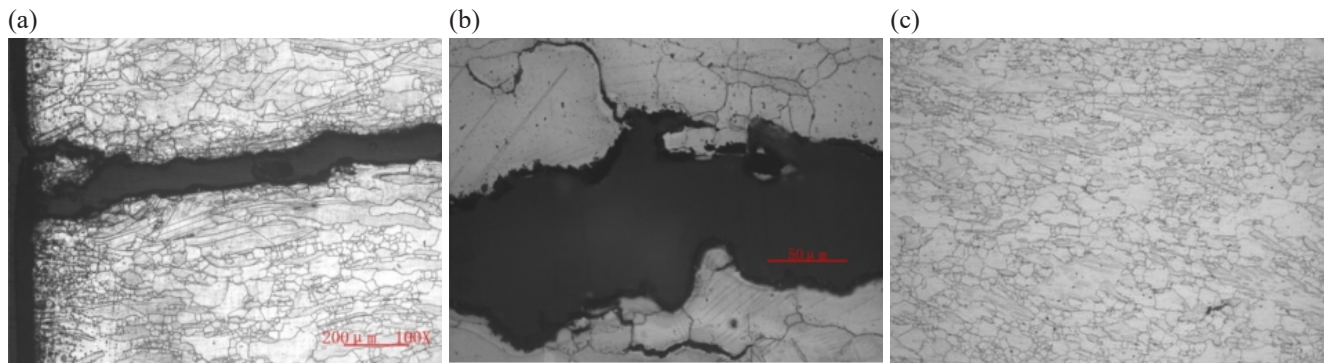
Figure 5. Metallographic analysis. **(a)** Initial cracking zone; **(b)** Expansion area; **(c)** Metallographic structure at normal position

2.5. Hardness inspection

The sample was cut near the crack for the Brinell hardness test, and the results are presented in **Table 1**. The hardness exhibited uniformity, with an average hardness of HB86, meeting the design requirement of HB260.

Table 1. Brinell hardness test results (HB2.5/62.5)

1	2	3	Average value
85	86	87	86

3. Analysis and discussion

The forging cracks are oriented parallel to the forging flow line and propagate from the external to the internal regions. They exhibited evenness, devoid of metallurgical defects, with the original crack area appearing dark gray, locally yellowish-brown, and the artificially interrupted fracture appearing silver-gray. The initial cracking zone of the crack was covered with more oxidation products, displaying distinct layered cracking and intergranular fracture characteristics. The expansion zone fracture is intergranular, with visible oxidation on the crystal surface, while the artificial interrupted fracture exhibits quasi-cleavage characteristics.

In summary, it is deduced that the forging cracking is intergranular and brittle. The structure near the crack consists of elongated deformed grains and a few fine equiaxed crystals, with a visible deformation zone, indicating a low degree of recrystallization. The main factors influencing recrystallization include the original material structure, deformation rate, and deformation temperature. The degree of recrystallization away from the crack is higher than at the crack location, suggesting that the main factors affecting recrystallization at the crack location may be a rapid deformation rate or low deformation temperature during forging. However, a rapid forging deformation rate may increase the number of crystal twinning, resulting in a higher hardness value
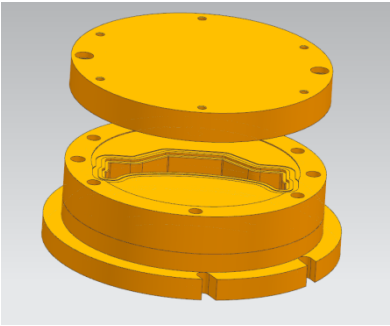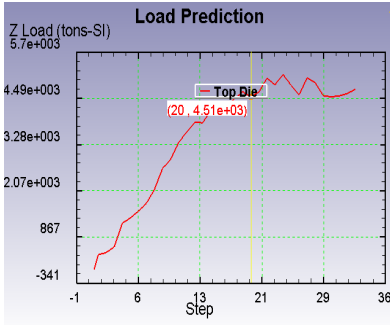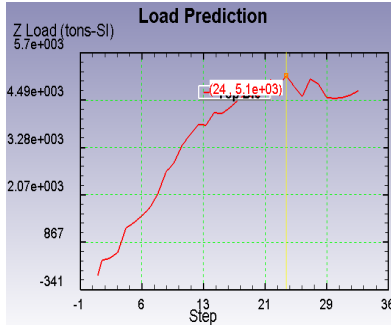
in positions with more twins [2]. Oxidation products are observed in the initial zone of crack fracture, indicating that the crack occurred before surface treatment. Additionally, only oxidation characteristics are evident inside the crack fracture, supporting the belief that the crack originated during the forging stage.

The deformation process of magnesium alloy primarily involves dislocation slip and twinning. Dislocation slip is hindered by grain boundaries, second phases, twin boundaries, etc., resulting in increased dislocation density within the magnesium alloy. At high temperatures, the dislocation with high density can induce recrystallization, resulting in grain refinement of magnesium alloy. Fine grains are easy to slip along grain boundaries and coordinate deformation. Dislocation at high temperatures makes it easier to slip or climb with less resistance [3]. Therefore, the magnesium alloy is conducive to promoting deformation at high temperatures. When the forging temperature is relatively low, the degree of dynamic recrystallization is weak, resulting in incomplete dynamic recrystallization, un-recrystallized structure, and hindered dislocation climbing. Subsequent deformation processes result in dislocation blockage at the grain boundary, initiating microcracks. The connection of microcracks ultimately leads to forging cracks along the crystal. Thus, the primary cause of cracking is the low forging temperature.

4. Simulation analysis

A simulation analysis was conducted on the forging mold with the mold structure detailed in **Table 2**. During forging, the blank is positioned in the lower mold, and upon the initiation of the upper mold's downward movement, the blank takes shape, reaching the desired displacement. The simulation analysis employed finite element software, and the parameters are outlined in **Table 3**. The design requirements specify that the forging process must be devoid of defects such as incomplete filling and folding, with the forging tonnage not exceeding 6000 T (in line with the equipment capacity of 6000 T).

**Table 2.** Mold structure and forming tonnage diagram

Mold structure diagram	Forming tonnage

Table 3. Simulation parameter diagram

Project	Temperature (℃)	Number of grids	Follow mold displacement	Step count
Blank	340	106,440		
Upper mold	350	115,020	0.35 mm	20
Lower mold	350	102,760		

Upon physical inspection (refer to **Table 4**), it is evident that during secondary forging, the material flows to both sides, and the forging fibers follow a horizontal direction. The low temperature of the blank induces the initiation of forging cracks along the fiber direction, aligning with the results observed in the metallographic analysis.

Table 4. Blank flow diagram
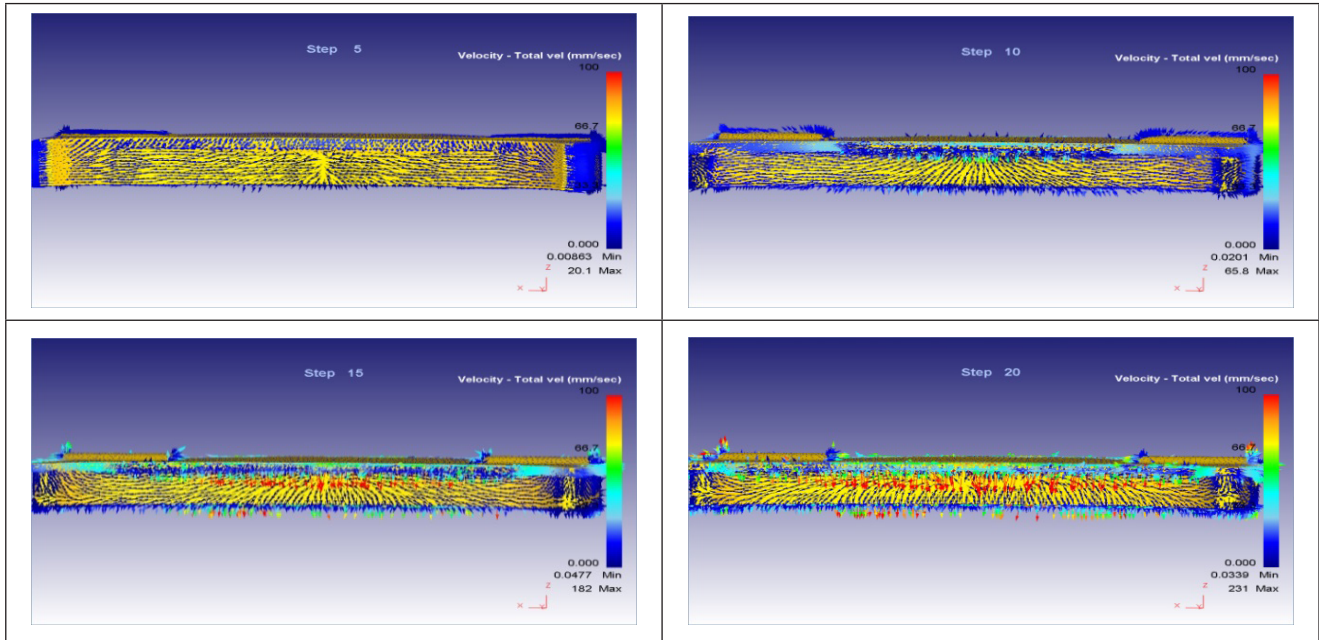
5. Conclusions

The cracking property of the part is intergranular brittle cracking. The recrystallization structure of the cracking part is not complete, which is related to the low forging temperature in the forging process.

Authors contribution

Funding acquisition, **Liying Jin**; Supervision, **Dongmei Liu**, **Jie Yuan**, **Ruihuan Tian**; Validation, **Lulu Song**.

Funding

Disclosure statement

The authors declare no conflict of interest.

References

[1] Editorial Committee of China Aviation Materials 2002, China Aviation Materials Handbook, Vol. 3, Aluminum Alloy,

Magnesium Alloy. 2nd Edition, China Standards Press, Beijing.

[2]   Dai L, Zhang R, Liu X, 2007, The Effect on Structure and Mechanics Property of MB15 Magnesium Alloy Deformation. Inner Mongolia Petrochemical Industry, 2007(11): 59–60.

[3]   Xiang J, Wang C, Chen K, et al., 2019, Surface Modification and Corrosion Resistance of MB15 Magnesium Alloy for Automobiles. Heat Treatment of Metals, 44(12): 186–192.